Noninvasive diffuse optical measurement of blood flow and blood oxygenation for monitoring radiation therapy in patients with head and neck tumors: a pilot study

Ulas Sunar
University of Pennsylvania
Department of Physics and Astronomy
209 South 33rd Street
Philadelphia, Pennsylvania 19104-6396

Harry Quon
University of Pennsylvania
Department of Radiation Oncology
Philadelphia, Pennsylvania 19104

Turgut Durduran
University of Pennsylvania
Department of Physics and Astronomy
209 South 33rd Street
Philadelphia, Pennsylvania 19104-6396

Jun Zhang
Juan Du
University of Pennsylvania
Department of Biochemistry and Biophysics
Philadelphia, Pennsylvania 19104

Chao Zhou
Guoqiang Yu
Regine Choe
University of Pennsylvania
Department of Physics and Astronomy
209 South 33rd Street
Philadelphia, Pennsylvania 19104-6396

Alex Kilger
Robert Lustig
Laurie Loevner
University of Pennsylvania
Department of Radiation Oncology
Philadelphia, Pennsylvania 19104

Shoko Nioka
Britton Chance
University of Pennsylvania
Department of Biochemistry and Biophysics
Philadelphia, Pennsylvania 19104

Arjun G. Yodh
University of Pennsylvania
Department of Physics and Astronomy
209 South 33rd Street
Philadelphia, Pennsylvania 19104-6396

Abstract. This pilot study explores the potential of noninvasive diffuse correlation spectroscopy (DCS) and diffuse reflectance spectroscopy (DRS) for monitoring early relative blood flow (rBF), tissue oxygen saturation (StO_2), and total hemoglobin concentration (THC) responses to chemo-radiation therapy in patients with head and neck tumors. rBF, StO_2, and THC in superficial neck tumor nodes of eight patients are measured before and during the chemo-radiation therapy period. The weekly rBF, StO_2, and THC kinetics exhibit different patterns for different individuals, including significant early blood flow changes during the first two weeks. Averaged blood flow increases $(52.7 \pm 9.7)\%$ in the first week and decreases $(42.4 \pm 7.0)\%$ in the second week. Averaged StO_2 increases from $(62.9 \pm 3.4)\%$ baseline value to $(70.4 \pm 3.2)\%$ at the end of the second week, and averaged THC exhibits a continuous decrease from pretreatment value of (80.7 ± 7.0) $[\mu M]$ to (73.3 ± 8.3) $[\mu M]$ at the end of the second week and to (63.0 ± 8.1) $[\mu M]$ at the end of the fourth week of therapy. These preliminary results suggest daily diffuse-optics-based therapy monitoring is feasible during the first two weeks and may have clinical promise. © *2006 Society of Photo-Optical Instrumentation Engineers.* [DOI: 10.1117/1.2397548]

1 Introduction

Head and neck cancer refers to malignancies arising from the mucosal surfaces of the oral cavity, pharynx, nasal cavity, and sinuses. Often these tumors metastasize to lymph nodes in the neck. Several methods for treatment of head and neck cancer are used including surgery, radiation therapy (RT), chemotherapy, and combinations thereof.[1] The vast majority of head and neck cancers are squamous cell carcinomas (SCC) and

Address all correspondence to Ulas Sunar, Univ. of Pennsylvania, UPenn, 209 S. 33rd St., Philadelphia, PA 19104; E-mail: sunar@sas.upenn.edu. Tel: 215-898-6833; Fax: 215-573 6391

treatment for this type of cancer, especially when locally advanced, often uses radiation therapy.

Radiation therapy efficacy is known to be dependent on oxygen status.[2] Therapeutic treatment is less efficacious in patients with poorly vascularized/hypoxic tumors, and it is therefore desirable to identify and target such patients for special treatment.[1,3,4] To date, some correlations between oxygenation status in human solid tumors and tumor response to therapy have been evaluated,[5] but the mechanisms associated with tumor oxygenation and blood flow variation during chemo-radiation are poorly understood.[6] Studies including head and neck carcinoma have exhibited an increase of positive response in tumors with high pretreatment oxygenation compared to poorly oxygenated tumors.[6,7] However, in these studies some well-oxygenated tumors failed to respond, while some hypoxic tumors responded, possibly due to changes in tumor oxygenation *during* treatment. One factor that modulates tumor tissue oxygenation is blood flow. Recent magnetic resonance imaging (MRI) and computed tomography (CT) investigations have demonstrated significant blood flow changes *during* therapy and have suggested that these early blood flow changes may have prognostic value.[8–10] Clearly functional assessment of blood oxygenation and flow variation during the early weeks of treatment holds potential for assessment of therapy efficacy/outcome. Moreover, blood flow and oxygenation changes during therapy may enable clinicians to adjust treatment dosage.

Several methods exist for measurement of oxygenation and blood flow. The oxygen-sensitive microelectrode needle method provides a "reference standard" for measurement of tumor oxygenation.[5,11] However it is invasive and inconvenient for clinical use.[12] Thus, there remains a need for reliable noninvasive techniques that measure tumor hemodynamic responses. Tumor blood flow measurements are particularly attractive for this application, since blood flow has been correlated with tumor oxygenation.[2,13,14] Blood flow has been measured in clinical studies by several imaging modalities, including positron emission tomography (PET),[12,15,16] dynamic computed tomography (CT),[10,17] dynamic contrast-enhanced magnetic resonance imaging (DCE-MRI),[8,9,18] MRI with spin labeling,[19] and ultrasound color Doppler.[20] Some of these techniques require contrast agent administration (PET, DCE-MRI) or ionizing radiation (CT); others are surface sensitive (laser Doppler),[21] and most are difficult to employ routinely with high throughput. The near-infrared diffuse optical methods presented here offer a noninvasive, rapid, portable, and low-cost alternative for repetitive bedside monitoring of tumor therapies.

The concept of noninvasive repetitive blood flow and oxygenation measurements is particularly attractive in the context of recent research on vascular modulating and antiangiogenic agents, which affect the response and sensitivity of tumors to chemotherapy and radiotherapy.[22–24] The work of Folkman[25] and other investigators, for example, has demonstrated potential therapeutic benefits of targeting tumor vasculature and tumor angiogenesis, and clinical trials of the anti-vascular endothelial growth factor (VEGF) monoclonal antibody bevacizumab have confirmed this new therapeutic paradigm.[26–29] To facilitate clinical translation of agents that target tumor vasculature, an ability to frequently assess tumor vessel blood flow and oxygenation with repetitive measurements is desir-

able, and potentially might lead to a means for individualized radiation therapy.

Diffuse optical spectroscopy and imaging has very recently emerged as a candidate for tumor therapy monitoring. In a case study, Jakubowski et al.[30] showed that the greatest breast tumor physiological (hemoglobin concentrations, water content, lipid content) changes occur within the first week of neoadjuvant chemotherapy. In a similar vein, combined diffuse optical imaging with ultrasound localization by Zhu et al.[31] demonstrated changes in the heterogeneous hemoglobin distribution in breast tumors during chemotherapy, and in a case study with comparison to DCE-MRI, Choe et al.[32] used the diffuse optical imaging technique to quantify optical contrast of breast tumors during chemotherapy.

In this contribution, we use noninvasive diffuse optical methods to investigate tumor responses to chemo-radiation therapy in a new class of patients with head and neck tumors. In contrast to previous work, our instruments concurrently incorporate diffuse correlation spectroscopy (DCS) as well as the more traditional diffuse reflectance spectroscopy (DRS). The DCS methodology permits assessment of tumor blood flow before and during radiation therapy, and the DRS measurements enable quantification of the concentration of tissue chromophores such as oxy- and deoxyhemoglobin. The DCS method detects moving blood cells, and has been successfully employed in animal studies,[33] for example, burn depth estimation in pigs[34] and cerebral blood flow in rats.[35,36,70] Very recently, the technique has been applied in human brain,[37,38] human muscle functional studies,[39] and in breast cancer patients.[40] Moreover, validation of DCS in some cases has been provided by comparison to the power Doppler ultrasound,[41] laser Doppler,[42] and arterial spin labeled MRI.[43] DRS provides information about oxygen saturation and total hemoglobin concentration and has been widely used in tumor and normal tissue functional studies.[44–52]

The investigation of a limited number of patients in this pilot study reveal that weekly relative blood flow (rBF), tissue oxygen saturation (StO_2), and total hemoglobin concentration (THC) kinetics exhibit different patterns for different individuals, including (on average) a significant early increase in rBF followed by a significant decrease in rBF. The averaged StO_2 exhibits an increase in the early weeks, while averaged THC tends to decrease continually during therapy.

2 Methods

2.1 Basic Principles of Diffuse Photon Correlation Spectroscopy

Near-infrared photons diffuse through thick living tissues.[33,53] When diffusing photons scatter from moving blood cells, they experience phase shifts that cause the intensity of detected light on the tissue surface to fluctuate in time. These fluctuations are more rapid for faster moving blood cells. Therefore, one can derive information about tissue blood flow far below the tissue surface from measurements of temporal fluctuations impressed on diffusing light.

Details of the diffuse photon correlation method can be found elsewhere.[34,35,54–56] Briefly, the normalized temporal intensity autocorrelation function of the diffused light,

$$g_2(r,\tau) = \frac{\langle I(r,t) \cdot I(r,t+\tau)\rangle}{\langle I\rangle^2}, \qquad (1)$$

is measured on the tissue surface. Here, $I(r,t)$ is the diffuse light intensity at position r, and time t, $\langle\ldots\rangle$ denotes a time average, and τ is the autocorrelation time delay. The electric field of the diffusing light $E(r,t)$ is also characterized by a temporal autocorrelation function, $G_1(r,\tau) = \langle E^*(r,\tau)E(r,t+\tau)\rangle$. Usually it is derived from measurements of $g_2(r,\tau)$ using the Siegert relation,[57] $g_2(r,\tau) = 1 + \beta|G_1(r,\tau)|^2/\langle I\rangle^2 = 1 + \beta|g_1(r,\tau)|^2$; here β is a constant that depends on source and detection experimental parameters such as the number of detected speckles, and $g_1(r,\tau) = G_1(r,\tau)/\langle I\rangle$ is the normalized field correlation function.

The electric field autocorrelation function traveling through dynamic turbid media obeys a diffusion equation.[34,54,58] Data collected in the reflectance geometry are readily analyzed by solving this diffusion equation using, for example, the semi-infinite medium approximation.[59] The analytical form of the autocorrelation function within the semi-infinite approximation can be obtained from the image source approach following Kienle and Patterson.[60] In particular, for semi-infinite homogeneous fluctuating turbid medium and for point sources of the form $S(r) = S_0\delta(r)$, the electric field autocorrelation function on the tissue surface is

$$G_1(r,\tau) = \frac{3\mu_s' S_0}{4\pi}\left[\frac{\exp(-kr_1)}{r_1} - \frac{\exp(-kr_2)}{r_2}\right], \qquad (2)$$

where $k^2 = 3\mu_s'\mu_a + 6\mu_s'^2 k_o^2\Gamma\tau$. Here, μ_a, μ_s' are the average absorption and scattering coefficients of the underlying medium. These can be obtained from DRS measurements, k_o is the wavenumber of light in the medium, and $r_1(r_2)$ is the distance between source (image source) and the detector on the surface. Detailed explicit forms of these solutions are given in the Appendix. $\Gamma = \alpha D_B$ characterizes temporal fluctuations in the medium due to scatterer motions such as blood flow. Here, α is a factor representing the probability that a scattering event in tissue is from a moving scatterer such as a red blood cell. It is proportional to tissue blood volume fraction. D_B is an "effective" diffusion coefficient for the blood cells. It should be noted that the effective diffusion coefficient need not (and is generally not) be the "thermal" Brownian motion predicted by Einstein;[61] nonthermal random forces in the vasculature can also give rise to diffusive particle motions. It is assumed herein that measured relative changes of αD_B are proportional to relative changes in tissue blood flow. Larger Γ implies faster electric field (or intensity) autocorrelation function temporal decay and higher blood flow (Fig.1). A detailed microscopic model relating tissue blood flow to Γ is not available; it is the subject of current research. Nevertheless, the proportional relationship has been verified[41–43] against a variety of traditional blood flow/perfusion measurement methods in a variety of different physiological contexts. We adopt this relationship as a fundamental assumption in our experimental approach. We note here that another related microscopic interpretation, which takes "bulk" blood displacement into account, explicitly has been proposed recently in the context of laser Doppler flowmetry.[62,63]
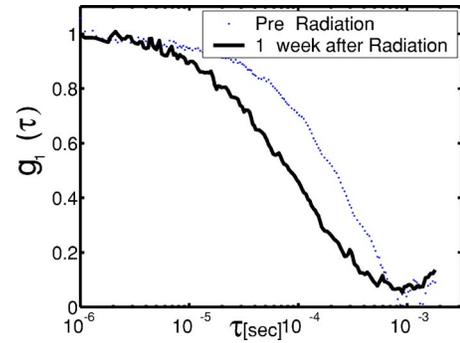

Fig. 1 Normalized temporal diffuse electric field autocorrelation function $[g_1(r,\tau) = G_1(r,\tau)/\langle I\rangle]$ data for patient 2 (P-2) before, and 1 week after radiation therapy. The faster temporal decay in the autocorrelation curve corresponds to an increased blood flow.

Using the Nelder-Mead Simplex algorithm in Matlab (Mathwork, Inc.) software, the flow parameter Γ and the experimental constant β are obtained by minimizing the difference between the predicted analytical form of the autocorrelation function in the reflectance geometry $g_{1,th}(r,\tau_i)$, and the measured autocorrelation function $g_{1,\exp}(r,\tau_i)$, i.e., $\chi^2 = \Sigma_i[g_{1,th}(r,\tau_i) - g_{1,\exp}(r,\tau_i)]^2$. The exact form of the autocorrelation function depends on measurement geometry as well as on tissue optical properties. Here we report rBF. rBF is a blood flow index defined as the blood flow parameter (Γ) relative to its pretreatment value (in percent units with 100% implying no change). rBF is thus unitless.

2.2 Blood Oxygen Saturation and Total Hemoglobin Concentration Measurements

The concentrations of oxy-, deoxy-, and total hemoglobin (C_{HbO_2}, C_{Hb}, THC), are extracted using DRS data with multiwavelength (λ) and multisource/detector separations (ρ). A multiwavelength fitting algorithm was applied to directly extract C_{Hb}, C_{HbO_2}, and the scattering coefficient, assuming an absorption due only to oxy- and deoxyhemoglobin, $\mu_a = \Sigma_i\varepsilon_i C_i$ ($i = Hb, HbO_2$). Here, ε_i is the extinction coefficient of the i'th chromophore at a given wavelength and is obtained from the literature.[64] It is also assumed that scattering follows a Mie-type behavior[65] in the near-infrared spectral window, i.e., $\mu_s' = A\lambda^{-B}$. We showed previously with simulations that fixing B allows more robust fitting with our multiwavelength fitting algorithm.[66] There are very few quantitative measurements of parameter B and its value ranges between 0.3 and 1.5.[67–69] We assumed a value of $B = 0.8$. Varying this value by 50% resulted in less than 5% variation in the quantification of scattering coefficients and other physiological parameters. In the analysis, we minimized $\chi^2 = \Sigma_\lambda\Sigma_\rho|R_m(\rho,\lambda,\mu_a,\mu_s') - R_c(\rho,\lambda,\mu_a,\mu_s')|^2$ to extract hemoglobin concentrations and A. R_m is the measured diffuse reflectance and R_c is the calculated diffuse reflectance in the semi-infinite geometry. An explicit form for R_c is given in the Appendix. After obtaining oxy- and deoxyhemoglobin concentrations, one readily derives total hemoglobin concentration THC, and blood oxygen saturation StO_2: $THC = C_{Hb} + C_{HbO_2}$ and $StO_2 = [C_{HbO_2}/THC] \times 100$. We have tested the multiwavelength
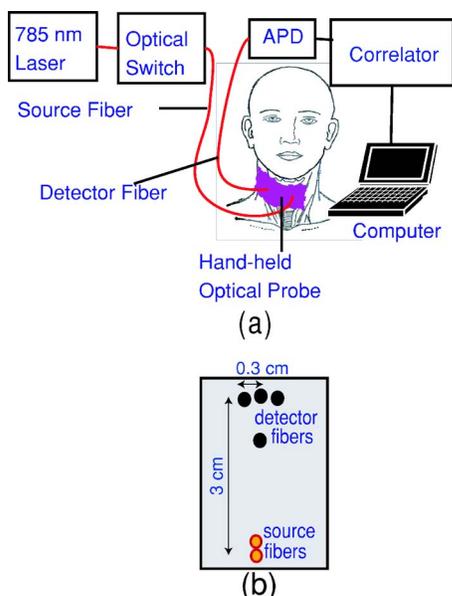
Fig. 2 (a) Diagram of the flow instrument (only one source fiber and one detector channel is shown for simplicity). The instrument consists of a 785-nm coherent laser, an optical switch, photon-counting avalanche photodiodes (APDs), and an autocorrelator board. The data are stored in a computer for postprocessing. (b) Hand-held optical probe: source and detector fibers are inserted into a soft pad. The maximum source detector separation is 3 cm.

Fig. 3 (a) Diagram of the frequency-domain instrument. Laser diodes (LD1,LD2,LD3) were modulated with 70-MHz rf signal. Two 1×4 optical switches were used to switch the colors and source fiber positions. The light was collected by two APDs and two PMTs (only one source, one detector fiber, and one channel of the instrument is shown for simplicity). (Amp=amplifier, BPF=bandpass filter, LPF=low-pass filter, IQ=in-phase and quadrature demodulators, and A/D=analog-to-digital converter.) (b) Optical probe: two detector fiber bundles and four source fibers are arranged with shortest separation of 1.8 cm, and longest separation of 3 cm. S1, S2, S3, and S4 are source fibers and Dl and D2 are detector fibers.

and multidistance fitting algorithm extensively with Intralipid titration, and we have found good correlation between extracted and expected optical properties.

2.3 Instrumentation

2.3.1 Diffuse correlation spectroscopy instrument

We constructed a portable four-channel system for use in the clinical study [Fig. 2(a)]. The instrument used a long coherence length laser (Crysta Laser, Nevada) operating at 785 nm, an optical switch (DiCon Fiberoptics, California), four photon-counting fast avalanche photodiodes (Perkin-Elmer, Canada), and a custom built four-channel autocorrelator board (Correlator.com, New Jersey). The source light delivered to the neck was switched between two multimode source fibers. Single-mode detector fibers were used to collect the light. All fibers were inserted into a soft pad so the operator could place this single hand-held probe onto the patient's neck [Fig. 2(b)]. Photons transmitted into the neck were collected by the single-mode detector fibers in reflectance. The shortest and largest separations between source and detector fibers were 2 and 3 cm, respectively. When our signals were small, we increased the number of fibers at large separations to increase the measurement signal-to-noise (SNR) ratio.[70] In the fitting process, the largest separation (3 cm) was used to extract blood flow parameters. Typically the average photon penetration depth into the tissue is one-third to one-half of the source-detector separation;[71,72] thus, we believe the signal originates largely from superficial neck tumor nodes.
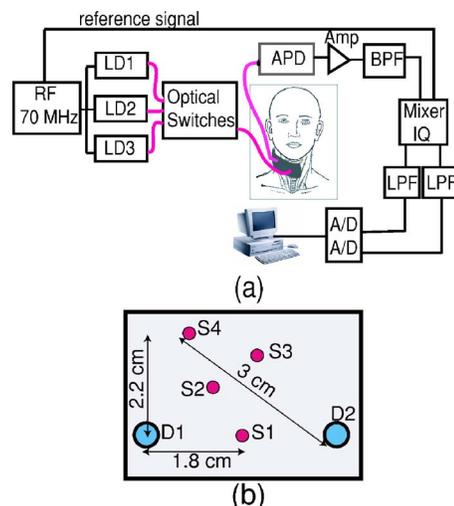
2.3.2 Diffuse reflectance spectroscopy instrument

A four-channel frequency domain instrument was used in the clinical study [Fig. 3(a)]. The details of the instrument are described elsewhere.[73,74] Briefly, the instrument uses 690-, 785-, and 830-nm laser diodes (Thorlabs Incorporated, New Jersey), each of which were modulated at 70 MHz. Two 1 $\times 4$ optical switches (DiCon Fiberoptics, California) were used to switch the wavelength and source fiber positions. The light was collected by two avalanche photodetectors (APD, Hamamatsu, C5331-04) and two PMTs (R928, Hamamatsu), which were all coupled onto the tissue surface via 3-mm fiber bundles. After amplifying and filtering, signals from the detectors were mixed with a reference signal in an in-phase and in-quadrature (IQ) demodulator (Mini-Circuits, New York), thus generating the I and Q signal components. After the low-pass filter, the dc components of the I and Q signals were used to calculate the amplitude and phase of the diffuse photon density waves (DPDWs) that passed through the tissue. In the measurements, an optical probe using two detector fiber bundles and four source fibers were employed [Fig. 3(b)]. Source and detector fibers were arranged such that at least four different source detector separations (1.8, 2.2, 2.6, and 3 cm) were used for each patient to quantify oxygenation parameters with fidelity. To calibrate the unknown source-detector coupling and to normalize the instrument response, the symmetry of the source-detector fibers and an Intralipid solution with known optical properties were used (see the Appendix). The absorbance of the ink was determined and calibrated using an Ocean Optics spectrometer; for scattering, we used the well-known formula for Intralipid from the literature.[64]
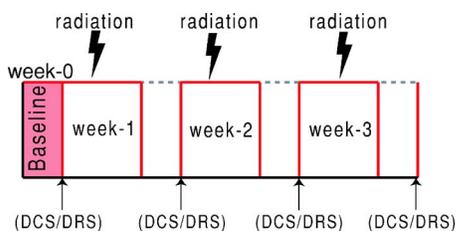
Fig. 4 Treatment and measurement schedule. See Methods in Sec. 2 for details.

2.4 Measurement Protocol

The study protocol was approved by the review board of human subjects of the University of Pennsylvania and informed consent was obtained from all patients. In our measurements, CT and MRI scans provided additional information about the location and size of each tumor. DCS and DRS measurements were carried out consecutively. The protocol (Fig. 4) consisted of preradiation measurements as baseline data. Subsequently, weekly measurements were carried out for each individual until his/her treatment was completed. Each patient received daily fractionated irradiation from Monday through Friday, and the optical measurements were completed just before treatment began each week. Patients were concurrently treated with weekly Carboplatin (area under the curve $=2$ mg/ml$\times$min) and Paclitaxel (30 mg/m^2). Daily fractionated radiotherapy was administrated with an intensity-modulated parotid-sparing radiotherapy technique. A simultaneous in-field boost prescription technique was used prescribing 7040 centiGray (cGy) in 220 cGy per fraction over 32 fractions to both primary and gross neck disease. The overall treatment time was about 6.4 weeks. Standard response evaluation criteria in solid tumors (RECIST)[75] response criteria was applied to classify tumor responses. A responder is defined as a patient with no evidence of residual cancer in the neck dissection specimen at the end of treatment. Formal assessment of treatment response was conducted 6 weeks after completing therapy. Postchemoradiotherapy neck dissections were evaluated using pathologic response.

The optical measurements were carried out by three different operators to assess the repeatability of the method. Each operator placed the probe onto the neck and arm muscle (for control purposes) three times. The data reported in this work represent an average ($\pm$ standard error) of the three operator measurements. Placement of the probe and consecutive measurements of both blood flow and oxygenation took $\sim$15 min in total, including the different observers. The largest nodal mass was selected for weekly optical measurements. Palpation and measurements with a ruler were the main tools used for identifying tumors during therapy. A trained radiology nurse was present during each measurement to assist in the identification of tumors. Tumor locations were measured with the ruler and systematically noted with respect to the ear and chin of the patients. Diffuse optical measurements placed the probe at the same center location of each tumor, and the measurements were repeated at that particular location. The repeatability error was small ($\sim$5%). No obvious trends with respect to operators were found. Only the diffuse optical method was available for weekly measurements. Structural images such as from CT were available at pretherapy only.

2.5 Statistical Analysis

All statistical analyses were performed using Matlab (Mathwork, Incorporated). Nonparametric procedures were applied, because of some deviations from a normal distribution. Paired comparisons were performed using the Wilcoxon (Mann-Whitney U) test, two-tailed, to identify trends and substantial changes. Differences were considered significant for $p \leq 0.05$.

3 Results

A total of eight patients were examined weekly. The patient and tumor characteristics are given in Table 1. Tables 2–4 summarize data from tumor (t) and arm muscle (m) of eight

Table 1 Characteristics of patients with head and neck cancer (SCC=squamous cell carcinoma, TNM =tumor, node, metastasis stage[76]).

Patient number	Age/Sex	Histologic type	TNM stage	Size/depth (cm)	Treatment response
P-1	68/F	SCC	$T_{4b}N_2M_0$	5.4 × 3.7/0.4	Complete
P-2	66/F	SCC	$T_1N_{2b}M_0$	5.0 × 3.2 /0.3	Complete
P-3	61/M	SCC	$T_{4a}N_1M_0$	2.5 × 2.0 /0.5	Complete
P-4	63/M	SCC	$T_2N_{2b}M_0$	3.6 × 3.1 /0.5	Complete
P-5	50/M	SCC	$T_2N_{2c}M_0$	3.8 × 4.1 /0.4	Complete
P-6	74/M	SCC	$T_4N_{2c}M_0$	5.1 × 4.0/0.6	Complete
P-7	63/M	SCC	$T_xN_{2a}M_0$	4.8 × 2.8 /0.3	Complete
P-8	49/M	SCC	$T_{4b}N_{2b}M_0$	5.5 × 4.5 /0.4	Partial

Table 2 Weekly relative blood flow changes (rBF[%]) of individual tumor (t) and arm muscle (m) tissue at the end of week 1, 2, 3, and 4 of chemo-radiation therapy. The pretreatment value at week 0 was defined as 100% in all patients. For patient 2 (P-2), optical measurements were stopped at the end of the third week, since the tumor was not palpable anymore. For patient 3 (P-3), optical measurements could not be acquired after the third week of therapy because of scheduling difficulties.

Patient number	Tissue type	Week 1 [%]	Week 2 [%]	Week 3 [%]	Week 4 [%]
P-1	t	152±5	135±9	98±3	120±9
P-1	m	103±7	119±6	104±6	112±4
P-2	t	167±6	110±11	108±6	-
P-2	m	97±20	83±9	80±12	-
P-3	t	150±11	98±10	118±16	-
P-3	m	111±14	91±10	119±17	-
P-4	t	199±15	92±33	71±42	79±34
P-4	m	65±15	66±10	62±10	63±4
P-5	t	148±12	134±12	185±20	189±14
P-5	m	83±14	81±14	100±22	105±18
P-6	t	117±4	113±9	104±9	116±8
P-6	m	113±18	94±11	87±11	109±10
P-7	t	136±15	90±5	183±8	95±14
P-7	m	77±9	90±18	94±8	92±14
P-8	t	116±9	144±16	197±29	270±17
P-8	m	111±5	81±7	79±10	74±5

Table 3 Weekly blood oxygen saturation (StO_2) [%] during chemo-radiation therapy for both tumor (t) and arm muscle (m) tissue.

Patient number	Tissue type	Week 0 [%]	Week 1 [%]	Week 2 [%]	Week 3 [%]	Week 4 [%]
P-1	t	56±4	53±4	59±2	48±4	48±3
P-1	m	57±4	58±1	60±1	58±3	59±3
P-2	t	76±9	71±2	74±2	66±2	-
P-2	m	68±4	69±5	68±3	65±2	-
P-3	t	50±3	78±4	79±2	73±6	-
P-3	m	56±4	55±4	55±3	56±5	-
P-4	t	70±6	71±2	74±3	71±4	78±11
P-4	m	60±3	59±3	58±2	67±2	65±3
P-5	t	58±5	67±4	75±3	67±10	75±2
P-5	m	58±3	59±2	58±2	56±1	50±4
P-6	t	62±3	56±2	58±3	67±6	54±2
P-6	m	63±4	69±2	64±2	75±3	62±3
P-7	t	68±3	67±3	74±2	67±3	57±8
P-7	m	66±2	61±7	62±4	67±4	57±3
P-8	t	67±5	69±4	73±4	76±3	76±2
P-8	m	73±4	76±4	75±3	78±2	78±4

patients (labeled P-1, P-2, …P-8). Table 2 exhibits rBF [%] at the end of week 1, week 2, week 3, and week 4 of chemo-radiation therapy. The pretreatment value at week 0 was defined as 100% in all patients. Similarly, Tables 3 and 4 summarize weekly changes of StO_2 [%] and THC [μM], respectively. For patient 2 (P-2), optical measurements were stopped at the end of third week because the tumor was no longer palpable. For patient 3 (P-3), optical measurements could not be acquired after the third week of the therapy because of scheduling difficulties. It is clear from the tables that our individual results varied greatly. This has also been the case in animal experiments[16] and clinical trials[2] employing radiation therapy; apparently, this variation is only partly a result of methodological factors such as differences in probe handling and positioning on the tissue.

A representative optical response of one of the complete responders is given in Fig. 5 (corresponding to P-l). In this case, rBF increased in the early weeks, and a subsequent decrease followed; StO_2 exhibited a small decrease with a subsequent small increase at the second week; and THC exhibited a continuous drop-off during therapy. Patient 8 (P-8), a

partial responder, was excluded from the statistical analysis, since P-8 exhibited substantially different tumor hemodynamic response during the therapy (Fig. 6); in this case rBF exhibited a continual increase, while StO_2 and THC also tended to increase over the course of treatment. For this patient, pretherapy CT showed a large necrotic nodal mass measuring ~5 cm diam, and the tumor was still relatively large and palpable at the end of the therapy. Postsurgical pathology confirmed the existence of residual tumor, and so the patient was considered to be a partial responder.

3.1 Average Relative Blood Flow Response

Figure 7 shows the trend of rBF, StO_2, and THC averaged over patients 1 to 7 (P-l, P-2, … P-7). A significant (p =0.0002) increase [(52.7±9.7)%] was observed in rBF during the first week of the therapy [Fig. 7(a)]. Our data also showed that tumor blood flow decreased [(42.4±7.0)%, p =0.007] during the second week of the therapy and remained low in the third and fourth weeks. The changes measured in the third (p=0.52) and fourth (p=0.92) weeks were not significant. Arm muscle levels had a tendency to decrease in the early weeks, but overall the changes were not statistically significant (p=0.54, 0.25, 0.30, and 0.19, respectively). Our observations are in reasonable agreement with other studies using different methods. Mantyla et al.[16] reported absolute blood flow changes in 43 patients (including squamous cell

Table 4 Weekly total hemoglobin concentration (THC) [μM] during chemo-radiation therapy for both tumor (t) and arm muscle (m) tissue.

| Patient number	Tissue type	Week 0 [μM]	Week 1 [μM]	Week 2 [μM]	Week 3 [μM]	Week 4 [μM]
P-1	t	82±4	77±4	74±3	66±5	51±5
P-1	m	73±9	70±7	75±6	69±5	64±5
P-2	t	53±5	42±5	40±4	43±3	-
P-2	m	58±14	56±14	54±8	45±3	-
P-3	t	75±16	81±20	97±12	50±15	-
P-3	m	70±6	70±3	65±9	61±8	-
P-4	t	75±10	94±15	80±10	74±12	63±15
P-4	m	80±6	73±6	80±8	82±4	81±6
P-5	t	76±8	56±7	51±6	39±6	40±8
P-5	m	104±17	116±5	113±10	103±6	112±8
P-6	t	90±2	85±3	99±7	96±4	92±4
P-6	m	86±8	80±3	82±5	84±10	80±10
P-7	t	114±9	94±18	72±11	87±6	64±14
P-7	m	73±8	70±17	74±7	60±11	67±11
P-8	t	30±6	40±8	30±7	37±9	50±7
P-8	m	45±6	47±9	53±9	49±8	56±10
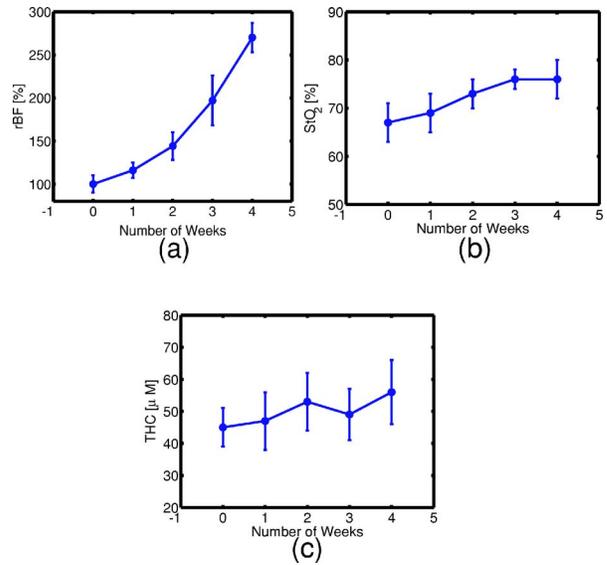
Fig. 6 (a) Tumor relative blood flow changes (rBF[%]) during chemo-radiation therapy for P-8. Pretreatment. value at week 0 was defined as 100%. Tumor (b) blood oxygen saturation (StO$_2$) and (c) total hemoglobin concentration (THC) during chemo-radiation therapy.

carcinoma of head and neck); a 56% (mean) increase at the end of the first week, and a statistically significant decrease was observed at the end of the second week using the ^{133}Xe clearance method. MRI studies have also reported an enhancement in blood flow after the first week of the therapy;[8,9,18,19,77] De Vries[9] quantified the blood flow changes and found a statistically significant increase of 21% after the first week and 25% after the second week of the radiation therapy in patients with rectal carcinoma.
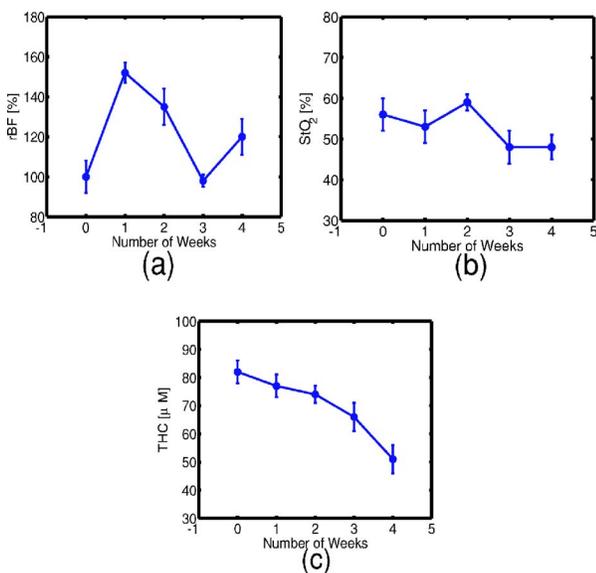

Fig. 5 (a) Tumor relative blood flow changes (rBF[%]) during chemo-radiation therapy for P-1. Pretreatment value at week 0 was defined as 100%. Tumor (b) blood oxygen saturation (StO$_2$) and (c) total hemoglobin concentration (THC) during chemo-radiation therapy.
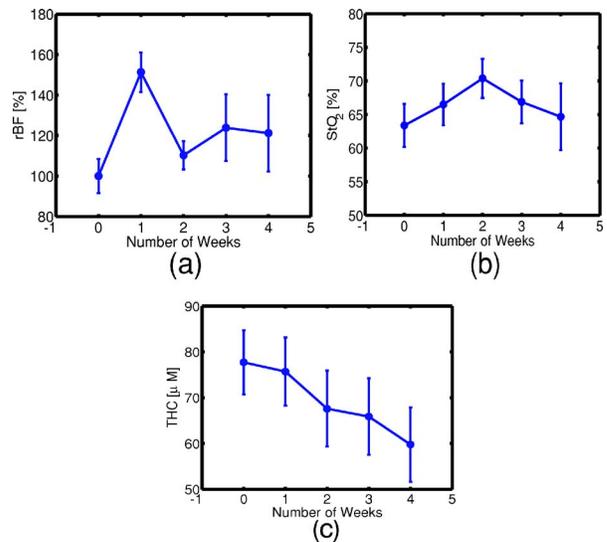

Fig. 7 (a) Tumor relative blood flow changes (rBF[%]) during chemo-radiation therapy averaged over all patients excluding P-8. Pretreatment value at week 0 was defined as 100% in all patients. (b) Average tumor blood oxygen saturation (StO$_2$) during chemo-radiation therapy. (c) Average tumor total hemoglobin concentration (THC) during chemo-radiation therapy.

The biologic significance of an increase in tumor blood flow is not well understood. It is possible that the increase may improve tumor oxygenation and therefore tumor radiosensitivity.[1,2,8] The mechanism for such a favorable response might be reflected in the observations of Sonveaux et al.[78] These investigators concluded that clinically relevant doses of radiation elicit a vascular stress response with increased secretion of tumor endothelial nitric oxide, which in turn can cause vasodilation, increased blood flow, and increased vessel permeability. Alternatively, this early increase in blood flow may reflect a corresponding decrease in the interstitial fluid pressure affecting the tumor vessel distensibility, and consequentially, blood flow.[79] Preferential damage to a subpopulation of oxygenated cells may lower the interstitial pressure on microvessels within the tumor, thus opening capillaries and increasing tumor blood microcirculation.[80] This effect can facilitate improved chemotherapy delivery to tumors as has been demonstrated in preclinical xenograft models.[81–83]

3.2 Average Tissue Oxygen Saturation Response

Average tumor StO_2 exhibited an increase in the first two weeks and a subsequent decrease [Fig. 7(b)]. The changes measured in the second ($p=0.006$) and third ($p=0.002$) weeks were significant, but those measured in the first ($p=0.08$) and fourth ($p=0.43$) weeks were not significant. The biggest difference from baseline [$(62.9 \pm 3.4)\%$] occurred at the end of the second week [$(70.4 \pm 3.2)\%$, $p=0.0003$]. The corresponding weekly arm muscle StO_2 levels gave $p=0.92, 0.58, 0.78, 0.03$, respectively. Preliminary work has suggested that tumor oxygenation response is dose dependent.[11,84] Small doses of radiation may facilitate an increased tumor oxygenation; however, relatively large doses of radiation can also damage tumor capillaries and reduce tumor oxygenation.[84] Clinical studies on tumor oxygenation *during* radiation are very scarce and are only limited to case reports.[11] Quantitative pO_2 measurements during the radiotherapy were first done by Badib and Webster.[85] At weekly intervals, a progressive increase in tumor oxygenation was observed. Bergsjo and Evans[86] reported a slight increase in the average oxygenation of tumors of the uterine cervix in the early phase (within 2 weeks) period of the therapy. In a recent study, 25 metastatic head and neck tumor nodes were investigated during chemoradiation therapy.[11] A clear increase was observed at the end of second week, and overall pO_2 values were decreased at the end of the therapy.

3.3 Average Total Hemoglobin Concentration Response

Average THC exhibited a continuous decrease during therapy [Fig. 7(c)]. Weekly changes ($p=0.40$, first week), ($p=0.15$, second week), ($p=0.72$, third week), ($p=0.47$, fourth week) were not statistically significant. The difference from baseline [$(80.7 \pm 7.0)\,[\mu M]$] to the end of the second week [$(73.3 \pm 8.3)\,[\mu M]$] was significant ($p=0.034$); however, the biggest difference from baseline occurred at the end of fourth week [$(63.0 \pm 8.1)\,[\mu M]$, $p=0.015$]. THC levels are related to tumor vascularity, and reduction of tumor vascularity after radiation and chemotherapy has been previously reported.[30,87,88] However, revascularization (neovasculariza-
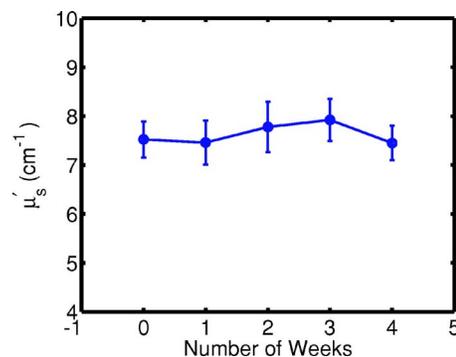

Fig. 8 Tumor scattering coefficient changes [$\mu_s'(\mathrm{cm}^{-1})$] during chemoradiation therapy for an average of patients P-1 to P-7.

tion) has also been observed in tumor tissue during radiation therapy.[16,21] Therefore, it should be noted that diffuse optical signals might be affected by combination of two opposing phenomena, resulting in fluctuations in individual THC levels during chemo-radiation therapy. Weekly arm muscle THC levels also changed, but not in a statistically significant fashion ($p=0.59, 0.80, 0.63, 0.40$, respectively). Arm THC levels had some tendency to decrease, possibly due to chemo-drugs, which may induce anemia.

3.4 Average μ_s' Changes

Weekly mean μ_s' for P1-P7 is plotted in Fig. 8. The results show $\sim 5\%$ variation in μ_s', suggesting that changes in functional parameters are more significant than changes in the structural parameter μ_s'.

4 Discussion

We have demonstrated the feasibility of diffuse optics for chemo-radiation therapy monitoring in head and neck cancer patients. In this section, we outline some of the limitations of the current approach. We also indicate variations in approach that will facilitate future improvement.

In our measurements, it is possible that different observers may have applied different probe-tissue pressure and introduced different probe positioning; both of these effects can induce variations in quantification. These variations were quantified and reported as error bars in the figures. In addition, the head and neck region consists of different anatomical tissues such as muscle and fat, which can vary across patients. Thus the semi-infinite homogeneous medium approximation is unlikely to be exactly valid. For example, our multidistance fitting scheme uses short separations ($\rho=1.8, 2.2, 2.6$ cm) and one long separation ($\rho=3$ cm). On the other hand, rBF was extracted using the longest separation ($\rho=3$ cm) only. Therefore, StO_2 and THC measurements are likely to be more affected by near surface tissues compared to blood flow measurements. Nevertheless, we have confined to employing the semi-infinite approximation because it simplifies our analysis enormously and enables us to extract trends from our weekly measurements. Better quantification, as well as increased ability to distinguish different tissue structure (tumor, muscle, fat), can be obtained from similar measurements using larger numbers of sources and detectors, and also by image segmen-

tation based on other available anatomical information.[31,89] However, in practice the larger number of sources and detectors also introduces some difficulty interfacing the probe to the tissue. From experience we have found that the relatively large probe having many fibers had disadvantages, especially when trying to contact all fibers to the tissue surface with equal pressure. Therefore, a bulkier single probe containing many blood flow and oxygen saturation fibers was avoided. In the future, a better probe design may enable better quantification by preserving good probe-tissue contact.

Additional benefits may be obtained by comparing the tumor to surrounding healthy tissue. Line scanning, as suggested by Jakubowski et al.,[30] across the tumor would be more favorable during therapy monitoring; however, it was not possible in our case due to time constraints. Ultimately, line scanning and/or imaging the whole tumor with rapid data acquisition should generate a richer dataset. Although radiation therapy science has improved with recent technological developments to better optimize beam localization in the tumor, normal tissue damage near the tumor may still exist. In the long term, it would be interesting to coregister radiated volume with the diffused photon path to better discriminate radiation effects on normal and tumor tissues.

Finally, limitations such as uncertainties in tumor boundaries can potentially be eliminated by coregistering the diffuse optical methods with other structural imaging modalities such as hand-held ultrasound[31] and MRI,[89,90] and by correcting for tumor shrinkage. Since CT is available only at pretherapy, adding a structural imaging methodology such as ultrasound into our protocol in the future would enable us to assess tumor size changes weekly, during therapy. Tissue heterogeneity effects may also be investigated with imaging techniques.[31,89]

In this study we have primarily focused on the *changes of hemodynamic responses* of the tumor as a result of a perturbation, i.e., chemo-radiation therapy. Because assessment of early response could potentially improve treatment outcome, the results we have presented encourage one to focus on early weeks. Indeed, as suggested by Jakubowski et al.,[30] one can carry out more frequent measurements (e.g., on a daily basis) to extract trends within the first week. It might even be interesting to focus on pretreatment conditions, possibly targeting patients for special protocols. In its current form, however, normalization of the blood flow to the first week precludes use of DCS before therapy begins. Extraction of absolute measures of blood flow will require better absolute calibration. In principle, DCS can be calibrated with other techniques at particular physiologic conditions, as was done recently with the MRI spin labeling technique,[43] but further work remains.

Our results suggest early clinical tumor response to radiation therapy can be detected and quantified by diffuse optical spectroscopies. The data clearly exhibit significant changes within two weeks of therapy. The early flow changes may be significant in affecting drug delivery efficacy and/or tumor oxygenation during chemo-radiation therapy, and the early tumor oxygenation changes may be related to tumor response. The responses of patients P-1 to P-7 were similar, and different from that of the partial responder patient P-8, but our statistics are not sufficient to draw significant physiological conclusions. Since a primary aim of therapy diagnostics is to predict the response as early as possible, the early blood flow and oxygenation changes observed here suggest the potential utility of daily measurements during the first two weeks of treatment. Due to very low accessibility of most other diagnostics methods, diffuse optical techniques have advantages for daily-based therapy monitoring.

5 Conclusion

Several techniques such as MRI, CT, and PET have been employed for monitoring tumor therapies, but the desire for a noninvasive, real-time bedside monitoring device makes diffuse optical techniques very attractive for clinical applications. Future clinical applications might also include concurrent use of optical methods with established modalities.[31,89,90]

With possible clinical requirements in mind, we quantify tumor rBF, StO_2, and THC changes noninvasively during chemo-radiation therapy using diffuse optical spectroscopies. These techniques do not require contrast agent administration and are suitable for bedside examinations with rapid data acquisition. Our preliminary data show that patients exhibit significant changes of rBF, StO_2, and THC, even in the first two weeks of treatment. In one patient (P-8), a different trend was observed with a preliminary indication that it coincided with a different treatment outcome. This anecdotal observation should be further studied with better statistics. At this point, more statistics are required for assessment of the prognostic value of these new methods. During treatment, different types of functional parameters may have different sensitivity to the therapy for different individuals. In other words, one parameter alone may not be a good predictor for a particular patient; multiparameter analyses such as those we present potentially enable clinicians to better discriminate and predict responses, and to continuously re-evaluate the treatment plan according to the probabilistic sensitivities of various hemodynamic functional parameters. Such experiments should be a next step.

APPENDIX

A.1 *Field Autocorrelation Function in Explicit Form*

It has been shown that the electric field autocorrelation function $G_1(r,\tau) = \langle E^*(r,t)E(r,t+\tau)\rangle$ in dynamic turbid media satisfies the steady-state diffusion equation:[34,54,58]

$$\nabla^2 G_1(r,\tau) - [3\mu_a \mu_s' + \alpha k_o^2 \mu_s'^2 \langle \Delta r^2(\tau)\rangle] G_1(r,\tau) = -3\mu_s' S(r).$$

(3)

$\langle \Delta r^2(\tau)\rangle$ is the mean squared displacement of the scatterers in the turbid medium in time interval τ. The exact form of the autocorrelation function depends on measurement geometry, tissue optical properties, as well as on the model that describes the nature of the scatterer motion. The mean squared displacement in the "effective" diffusion model is $\langle \Delta r^2(\tau)\rangle = 6D_B\tau$. In the main text we have set $\Gamma = \alpha D_B$. The mean squared displacement in the random flow model is $\langle \Delta r^2(\tau)\rangle = \langle v^2\rangle\tau^2$, where $\langle v^2\rangle$ is the mean square velocity of the scatterer in the vasculature. We adopt the effective diffusion model for our analysis.

For a point source $[S(r) = S_0 \delta(r)]$, the solution for a semi-infinite geometry can be obtained using an image source approach following Kienle and Patterson.[60] It is given by Eq. (2) in the main text, i.e.:

$$G_1(\rho, \tau) = \frac{3\mu'_s S_0}{4\pi} \left[\frac{\exp(-kr_1)}{r_1} - \frac{\exp(-kr_2)}{r_2} \right], \quad (4)$$

where $k^2 = 3\mu'_s \mu_a + 6\mu'_s 2k_0^2 \Gamma \tau$, $r_1 = \sqrt{\rho^2 + z_0^2}$ and $r_2 = [\rho^2 + (z_0 + 2z_b)^2]^{1/2}$. Here, ρ is the source-detector separation measured

along the tissue surface, z_0 is the effective depth of the source, $z_0 = \mu'^{-1}_s$, and z_b is the distance above the tissue surface at which fluence rate extrapolates to zero and is given by $z_b = 1.76/\mu'_s$ in case of the refraction indices of tissue and air: $n_{tissue} = 1.35$ and $n_{air} = 1.00$. The explicit form of the field autocorrelation function in semi-infinite geometry is:

$$G_1(\rho, \tau, \mu_a, \mu'_s) = \frac{3\mu'_s S_0}{4\pi} \left[\frac{\exp\left(- (3\mu'_s \mu_a + 6\mu'_s k_0^2 \Gamma \tau)^{\frac{1}{2}} \sqrt{\rho^2 + \mu'^{-2}_s}\right)}{\sqrt{\rho^2 + \mu'^{-2}_s}} \right.$$
$$\left. - \frac{\exp\left(- (3\mu'_s \mu_a + 6\mu'_s k_0^2 \Gamma \tau)^{\frac{1}{2}} \left\{\rho^2 + \left[\mu'^{-2}_s + 2\left(\frac{1.76}{\mu'_s}\right)^2\right]\right\}^{\frac{1}{2}}\right)}{\left\{\rho^2 + \left[\mu'^{-2}_s + 2\left(\frac{1.76}{\mu'_s}\right)^2\right]\right\}^{\frac{1}{2}}} \right]. \quad (5)$$

Note in our experiments that we often use the normalized field autocorrelation function $g_1(r, \tau) = G_1(r, \tau)/\langle I \rangle$.

A.2 Diffuse Reflectance in Explicit Form

The photon fluence rate also satisfies a diffusion equation. In the frequency domain and using a point source that is intensity modulated sinusoidally with modulation frequency ω

$[i.e., S_\omega(r, t) = S_0 \delta(r)\exp(i\omega t)]$, the time-independent diffusion equation for the photon fluence rate is:

$$D\nabla^2 \Phi_\omega(r) + (- v\mu_a + i\omega)\Phi_\omega(r) = vS_0 \delta(r), \quad (6)$$

where v is the speed of light and D is the diffusion coefficient of light in tissue. Using the image source approach as before, the explicit solution of the reflectance in semi-infinite geometry can be obtained and is:

$$R_c(\rho_{ij}, \lambda, \mu_a, \mu'_s) = \frac{3\mu'_s S_0 S_i D_j}{4\pi} \left(\frac{\exp\left\{ -\left[3\mu'_s\left(\frac{-i\omega}{v + \mu_a}\right)\right]^{\frac{1}{2}} \sqrt{\rho_{ij}^2 + \mu'^{-2}_s} \right\}}{\sqrt{\rho_{ij}^2 + \mu'^{-2}_s}} \right.$$
$$\left. - \frac{\exp\left(-\left[3\mu'_s\left(\frac{-i\omega}{v + \mu_a}\right)\right]^{\frac{1}{2}} \left\{\rho_{ij}^2 + \left[\mu'^{-2}_s + 2\left(\frac{1.76}{\mu'_s}\right)^2\right]\right\}^{\frac{1}{2}}\right)}{\sqrt{\rho_{ij}^2 + \left(\mu'^{-2}_s + 2\left(\frac{1.76}{\mu'_s}\right)^2\right)}} \right). \quad (7)$$

Here, ρ_{ij} is the distance between the i'th source and j'th detector, and $S_i D_j$ is the coupling coefficient for the i'th source and j'th detector pair.

Physics Division of Hospital of the University of Pennsylvania for providing CT, MRI, and PET scans of our head and neck patients.

References

1. H. J. Feldmann, M. Molls, and P. Vaupel, "Blood flow and oxygenation status of human tumors. Clinical investigations," *Strahlenther. Onkol.* **175**(1), 1–9 (1999).
2. P. Vaupel, F. Kallinowski, and P. Okunieff, "Blood flow, oxygen and nutrient supply, and metabolic microenvironment of human tumors: A review," *Cancer Res.* **49**(23), 6449–6465 (1989)
3. D. M. Brizel, G. S. Sibley, L. R. Prosnitz, R. L. Scher, and M. W. Dewhirst, "Tumor hypoxia adversely affects the prognosis of carcinoma of the head and neck," *Int. J. Radiat. Oncol., Biol., Phys.* **38**(2), 285–289 (1997).
4. A. Ressel, C. Weiss, and T. Feyerabend, "Tumor oxygenation after radiotherapy, chemotherapy, and/or hyperthermia predicts tumor free survival," *Int. J. Radiat. Oncol., Biol., Phys.* **49**(4), 1119–1125 (2001).
5. H. B. Stone, J. M. Brown, T. L. Philips, and R. M. Sutherland, "Oxygen in human tumors: Correlations between methods of measurement and response to therapy," *Radiat. Res.* **136**, 422–434 (1993).
6. H. Lyng, K. Sundfor, and E. K. Rofstad, "Changes in tumor oxygen tension during radiotherapy of uterine cervical cancer: Relationships to changes in vascular density, cell density, and frequency to changes in vascular density, cell density, and frequency of mitosis and apoptosis," *Int. J. Radiat. Oncol., Biol., Phys.* **46**(4), 935–946 (2000).
7. H. Lyng, T. Gunnar, J. F. Evensen, and E. K. Rofstad, "Changes in oxygen tension during radiotherapy of head and neck tumors," *Acta Oncol.* **38**(8), 1037–1042 (1999).
8. N. A. Mayr, W. T. Yuh, V. A. Magnotta, J. C. Ehrhardt, J. A. Wheeler, J. I. Sorosky, C. S. Davis, B. C. Wen, D. D. Martin, R. E. Pelsang, R. E. Buller, L. W. Oberley, D. E. Mellenberg, and D. H. Hussey, "Tumor perfusion studies using fast magnetic resonance imaging technique in advanced cervical cancer: a new noninvasive predictive assay," *Int. J. Radiat. Oncol., Biol., Phys.* **36**(3), 623–633 (1996).
9. A. F. DeVries, C. Kremser, P. A. Hein, J. Griebel, A. Krezcy, D. Ofner, K. P. Pfeiffer, P. Lukas, and W. Judmaier, "Tumor microcirculation and diffusion predict therapy outcome for primary rectal carcinoma," *Int. J. Radiat. Oncol., Biol., Phys.* **56**(4), 958–965 (2003).
10. R. Hermans, P. Lambin, A. Van der Goten, W. Van den Bogaert, B. Verbist, C. Weltens, and P. R. Delaere, "Tumoural perfusion as measured by dynamic computed tomography in head and neck carcinoma," *Radiother. Oncol.* **53**(2), 105–111 (1999).
11. L. W. Brady, H. P. Heilmann, and M. Molls, *Blood Perfusion and Microenvironment of Human Tumors*, Springer, Berlin (2000).
12. K. Lehtio, O. Eskola, T. Viljanen, V. Oikonen, T. Gronroos, L. Sillanmaki, R. Grenman, and H. Minn, "Imaging perfusion and hypoxia with PET to predict radiotherapy response in head-and-neck cancer," *Int. J. Radiat. Oncol., Biol., Phys.* **59**(4), 971–982 (2004).
13. J. Bussink, J. H. Kaanders, P. F. Rijken, J. A. Raleigh, and A. J. Van der Kogel, "Changes in blood perfusion and hypoxia after irradiation of a human squamous cell carcinoma xenograft tumor line," *Radiat. Res.* **153**(4), 398–404 (2000).
14. B. M. Fenton, E. M. Lord, and S. F. Paoni, "Effects of radiation on tumor intravascular oxygenation, vascular configuration, development of hypoxia, and clonogenic survival," *Radiat. Res.* **155**(2), 360–368 (2001).
15. S. L. Bacharach, S. K. Libutti, and J. A. Carrasquillo, "Measuring tumor blood flow with H(2)(15)O: Practical considerations," *Nucl. Med. Biol.* **27**(7), 671–676 (2000).
16. M. J. Mantyla, J. T. Toivanen, M. A. Pitkanen, and A. H. Rekonen, "Radiation-induced changes in regional blood flow in human tumors," *Int. J. Radiat. Oncol., Biol., Phys.* **8**(10), 1711–1717 (1982).
17. R. Hermans, P. Lambin, W. Van den Bogaert, K. Haustermans, A. Van der Goten, and A. L. Baert, "Non-invasive tumour perfusion measurement by dynamic CT: preliminary results," *Radiother. Oncol.* **44**(2), 159–162 (1997).
18. M. A. Rosen, H. Poptani, L. Loevner, D. Rosenthal, and J. Glickson, "Dynamic enhanced MRI of squamous cell carcinoma of the head and neck: predictors of early clinical response," Proc. 88th Ann. Mtg. RSNA (2002).
19. P. Schmitt, M. Kotas, A. Tobermann, A. Haase, and M. Flentje, "Quantitative tissue perfusion measurements in head and neck carcinoma patients before and during radiation therapy with a non-invasive MR imaging spin-labeling technique," *Radiother. Oncol.* **67**(1), 27–34 (2003).
20. J. P. Pirhonen, S. A. Grenman, A. B. Bredbacka, R. O. Bahado-Singh, and T. A. Salmi, "Effects of external radiotherapy on uterine blood-flow in patients with advanced cervical carcinoma assessed by color Doppler ultrasonography," *Cancer* **76**(1), 67–71 (1995).
21. N. G. Huilgol, M. M. Khan, and R. Puniyani, "Capillary perfusion–a study in two groups of radiated patients for cancer of head and neck," *Indian J. Cancer* **32**(2), 59–62 (1995).
22. R. K. Jain, "Normalizing tumor vasculature with anti-angiogenic therapy: a new paradigm for combination therapy," *Nat. Med.* **7**(9), 987–989 (2001).
23. R. K. Jain, L. L. Munn, and D. Fukumura, "Dissecting tumour pathophysiology using intravital microscopy," *Nat. Rev. Cancer* **2**(4), 266–276 (2002).
24. D. Hanahan and R. A. Weinberg, "The hallmarks of cancer," *Cell* **100**(1), 57–70 (2000).
25. J. Folkman, "Angiogenesis in cancer, vascular, rheumatoid and other disease," *Nat. Med.* **1**, 27–31 (1995).
26. C. G. Willett, Y. Boucher, E. di Tomaso, D. G. Duda, L. L. Munn, R. T. Tong, D. C. Chung, D. V. Sahani, S. P. Kalva, S. V. Kozin, M. Mino, K. S. Cohen, D. T. Scadden, A. C. Hartford, A. J. Fischman, J. W. Clark, D. P. Ryan, A. X. Zhu, L. S. Blaszkowsky, H. X. Chen, P. C. Shellito, G. Y. Lauwers, and R. K. Jain, "Direct evidence that the VEGF-specific antibody bevacizumab has antivascular effects in human rectal cancer," *Nat. Med.* **10**(2), 145–147 (2004).
27. D. H. Johnson, L. Fehrenbacher, W. F. Novotny, R. S. Herbst, J. J. Nemunaitis, D. M. Jablons, C. J. Langer, R. F. DeVore, J. Gaudreault, L. A. Damico, E. Holmgren, and F. Kabbinavar, "Randomized phase II trial comparing bevacizumab plus carboplatin and paclitaxel with carboplatin and paclitaxel alone in previously untreated locally advanced or metastatic non-small-cell lung cancer," *J. Clin. Oncol.* **22**(11), 2184–2191 (2004).
28. F. F. Kabbinavar, J. Schulz, M. McCleod, T. Patel, J. T. Hamm, H. J. Randolph, R. Mass, B. Perrou, B. Nelson, and W. F. Novotny, "Addition of bevacizumab to bolus fluorouracil and leucovorin in first-line metastatic colorectal cancer: results of a randomized phase II trial," *J. Clin. Oncol.* **23**(16), 3697–3705 (2005).
29. J. C. Yang, L. Haworth, R. M. Sherry, P. Hwu, D. J. Schwartzentruber, S. L. Topalian, S. M. Steinberg, H. X. Chen, and S. A. Rosenberg, "A randomized trial of bevacizumab, an anti-vascular endothelial growth factor antibody, for metastatic renal cancer," *N. Engl. J. Med.* **349**(5), 427–434 (2003).
30. D. B. Jakubowski, A. E. Cerussi, F. Bevilacqua, N. Shah, D. Hsiang, J. Butler, and B. J. Tromberg, "Monitoring neoadjuvant chemotherapy in breast cancer using quantitative diffuse optical spectroscopy: a case study," *J. Biomed. Opt.* **9**(1), 230–238 (2004).
31. Q. Zhu, S. H. Kurtzmany, P. Hegde, S. Tannenbaum, M. Kane, M. Huang, N. G. Chen, B. Jagjivan, and K. Zarfos, "Utilizing optical tomography with ultrasound localization to image heterogeneous hemoglobin distribution in large breast cancers," *Neoplasia* **7**(3), 263–270 (2005).
32. R. Choe, A. Corlu, K. Lee, T. Durduran, S. D. Konecky, M. Koptyra, S. R. Arridge, B. J. Czerniecki, D. L. Fraker, A. DeMichele, B. Chance, M. Rosen, and A. G. Yodh, "Diffuse optical tomography of breast cancer during neoadjuvant chemotherapy: a case study with comparison to MRI," *Med. Phys.* **32**(4), 1–11 (2005).
33. A. G. Yodh and D. A. Boas, *Biomedical Photonics*, Chap. 21, pp. 21/1-45, CRC Press, Boca Raton, FL (2003).
34. D. A. Boas and A. G. Yodh, "Spatially varying dynamical properties of turbid media probed with diffusing temporal light correlation," *J. Opt. Soc. Am. A* **14**(1), 192–215 (1997).
35. C. Cheung, J. P. Culver, K. Takahashi, J. H. Greenberg, and A. G. Yodh, "*In vivo* cerebrovascular measurement combining diffuse near-infrared absorption and correlation spectroscopies," *Phys. Med. Biol.* **46**, 2053–2065 (2001).
36. J. P. Culver, T. Durduran, D. Furuya, C. Cheung, J. H. Greenberg, and A. G. Yodh, "Diffuse optical tomography of cerebralblood flow, oxygenation, and metabolism in rat during focal ischemia," *J. Cereb. Blood Flow Metab.* **23**(8), 911–924 (2003).
37. T. Durduran, G. Yu, M. G. Burnett, J. A. Detre, J. H. Greenberg, J. Wang, C. Zhou, and A. G. Yodh, "Diffuse optical measurement of

blood flow, blood oxygenation, and metabolism in a human brain during sensorimotor cortex activation," *Opt. Lett.* **29**(15), 1766–1768 (2004).

38. J. Li, G. Dietsche, D. Iftime, S. E. Skipetrov, G. Maret, T. Elbert, B. Rockstroh, and T. Gisler, "Noninvasive detection of functional brain activity with near-infrared diffusing-wave spectroscopy," *J. Biomed. Opt.* **10**(4), 44002 (2005).

39. G. Yu, T. Durduran, G. Lech, C. Zhou, B. Chance, E. R. Mohler III, and A. G. Yodh, "Time-dependent blood flow and oxygenation in human skeletal muscle measured by noninvasive near-infrared diffuse optical spectroscopies," *J. Biomed. Opt.* **10**(2), 024027 (2005).

40. T. Durduran, R. Choe, G. Yu, C. Zhou, J. C. Tchou, B. J. Czerniecki, and A. G. Yodh, "Diffuse optical measurement of blood flow in breast tumors," *Opt. Lett.* **30**, 2915–2917 (2005).

41. G. Yu, T. Durduran, H. W. Wang, C. Zhou, H. M. Saunders, C. M. Sehgal, T. M. Busch, and A. G. Yodh, "Non-invasive monitoring of hemodynamic responses in RIF tumors during and after PDT," *Clin. Cancer Res.* **11**(9), 3543–3552 (2005).

42. T. Durduran, "Noninvasive measurements of tissue hemodynamics with hybrid diffuse optical methods," PhD Thesis, Univ. Pennsylvania (2004).

43. G. Yu, T. F. Floyd, T. Durduran, C. Zhou, J. J. Wang, J. M. Murphy, and A. G. Yodh, "Validation of diffuse correlation spectroscopy for muscle blood flow with concurrent arterial-spin-labeling perfusion MRI" (submitted for publication).

44. B. Chance, "Near-infrared images using continuous, phase-modulated, and pulsed light with quantitation of blood and blood oxygenation," *Ann. N.Y. Acad. Sci.* **838**, 19–45 (1998).

45. S. Srinivasan, B. W. Pogue, S. Jiang, H. Dehghani, C. Kogel, S. Soho, J. J. Gibson, T. D. Tosteson, S. P. Poplack, and K. D. Paulsen, "Interpreting hemoglobin and water concentration, oxygen saturation, and scattering measured *in vivo* by near-infrared breast tomography," *Proc. Natl. Acad. Sci. U.S.A.* **100**(21), 12349–12354 (2003).

46. B. J. Tromberg, N. Shah, R. Lanning, A. Cerussi, J. Espinoza, T. Pham, L. Svaasand, and J. Butler, "Non-invasive <emph type ="italic">in vivo</emph> characterization of breast tumors using photon migration spectroscopy," *Neoplasia* **2**(1-2), 26–40 (2000).

47. N. Shah, A. Cerussi, C. Eker, J. Espinoza, J. Butler, J. Fishkin, R. Hornung, and B. Tromberg, "Noninvasive functional optical spectroscopy of human breast tissues," *Proc. Natl. Acad. Sci. U.S.A.* **98**(8), 4420–4425 (2001).

48. R. Cubeddu, C. D'Andrea, A. Pifferi, P. Taroni, A. Torricelli, and G. Valentini, "Effects of the menstrual cycle on the red and near-infrared optical properties of the human breast," *Photochem. Photobiol.* **72**, 383–391 (2000).

49. D. T. Delpy and M. Cope, "Quantification in tissue near-infrared spectroscopy," *Philos. Trans. R. Soc. London* **352**, 649–659 (1997).

50. T. J. Farrell, M. S. Patterson, and B. Wilson, "A diffusion theory model of spatially resolved, steady state diffuse reflectance for the noninvasive determination of tissue optical properties <emph type ="italic">in vivo</emph>," *Med. Phys.* **19**, 879–888 (1992).

51. T. H. Foster, R. S. Murant, R. G. Byrant, R. S. Knox, S. L. Gibson, and R. Hilf, "Oxygen consumption and diffusion effects in photodynamic therapy," *Radiat. Res.* **126**, 296–303 (1991).

52. E. Gratton, S. Fantini, M. A. Franceschini, G. Gratton, and M. Fabiani, "Measurements of scattering and absorption changes in muscle and brain," *Philos. Trans. R. Soc. London* **352**(1354), 727–735 (1997).

53. A. Yodh and B. Chance, "Spectroscopy and imaging with diffusing light," *Phys. Today* **48**(3), 34–40 (1995).

54. D. A. Boas, L. E. Campbell, and A. G. Yodh, "Scattering and imaging with diffusing temporal field correlations," *Phys. Rev. Lett.* **75**(9), 1855–1858 (1995).

55. G. Maret and P. E. Wolf, "Multiple light scattering from disordered media, the effect of brownian motion of scatterers," *Z. Phys. B: Condens. Matter* **65**(1), 409–413 (1987).

56. D. J. Pine, D. A. Weitz, P. M. Chaikin, and E. Herbolzheimer, "Diffusing wave spectroscopy," *Phys. Rev. Lett.* **60**(12), 1134–1137 (1988).

57. B. J. Berne and R. Pecora, *Dynamic Light Scattering*, Wiley, New York (1976).

58. M. Heckmeier, S. E. Skipetrov, G. Maret, and R. Maynard, "Imaging of dynamic heterogeneities in multiple-scattering media," *J. Opt. Soc. Am. A* **14**(1), 185–191 (1997).

59. R. C. Haskell, L. O. Svaasand, T. Tsay, T. Feng, M. S. McAdams, and B. J. Tromberg, "Boundary conditions for the diffusion equation in radiative transfer," *J. Opt. Soc. Am. A* **11**, 2727–2741 (1994).

60. A. Kienle and M. S. Patterson, "Improved solutions of the steady-state and the time-resolved diffusion equations for reflectance from a semi-infinite turbid medium," *J. Opt. Soc. Am. A* **14**(1), 246–254 (1997).

61. A. Einstein, "On the motion of small particles suspended in liquids at rest required by the molecular-kinetic theory of heat," *Ann. Phys.* **17**, 549–560 (1905).

62. T. Binzoni, T. S. Leung, D. Rüfenacht, and D. T. Delpy, "Absorption and scattering coefficient dependence of laser-doppler flowmetry models for large tissue volumes," *Phys. Med. Biol.* **51**, 311–333 (2006).

63. R. Lohwasser and G. Soelkner, "Experimental and theoretical laser-doppler frequency spectra of a tissuelike model of a human head with capillaries," *Appl. Opt.* **38**(10), 2128–2137 (1999).

64. S. Prahl, "Optical properties spectra" (see http://omlc.ogi.edu/spectra/index.html) (2001).

65. J. R. Mourant, T. Fuselier, J. Boyer, T. M. Johnson, and I. J. Bigio, "Predictions and measurement of scattering and absorption over broad wavelength ranges in tissue phantoms," *Appl. Opt.* **36**, 949–957 (1997).

66. A. Corlu, R. Choe, T. Durduran, K. Lee, M. Schweiger, S. R. Arridge, E. M. C. Hillman, and A. G Yodh, "Diffuse optical tomography with spectral constraints and wavelength optimization," *Appl. Opt.* **44**(11), 2082–2093 (2005).

67. D. Grosenick, H. Wabnitz, K. T. Moesta, J. Mucke, P. M. Schlag, and H. Rinneberg, "Time-domain scanning optical mammography: II. Optical properties and tissue parameters of 87 carcinomas," *Phys. Med. Biol.* **50**(11), 2451–2468 (2005).

68. B. W. Pogue, S. Jiang, H. Dehghani, C. Kogel, S. Soho, S. Srinivasan, X. Song, T. D. Tosteson, S. P. Poplack, and K. D. Paulsen, "Characterization of hemoglobin, water, and NIR scattering in breast tissue: analysis of intersubject variability and menstrual cycle changes," *J. Biomed. Opt.* **9**(3), 541–552 (2004).

69. N. Shah, A. E. Cerussi, D. Jakubowski, D. Hsiang, J. Butler, and B. J. Tromberg, "The role of diffuse optical spectroscopy in the clinical management of breast cancer," *Dis. Markers* **19**(2–3), 95–105 (2003).

70. C. Zhou, G. Yu, F. Daisuke, J. H. Greenberg, A. G. Yodh, and T. Durduran, "Diffuse optical correlation tomography of cerebral blood flow during cortical spreading depression in rat brain," *Opt. Express* **14**, 1125–1144 (2006).

71. M. S. Patterson, S. Anderson, B. C. Wilson, and E. K. Osei, "Absorption spectroscopy in tissue-simulating materials: a theoretical and experimental study of photon paths," *Appl. Opt.* **34**(1), 22–30 (1995).

72. Y. S. Fawzi, A. M. Youssef, M. H. el Batanony, and Y. M. Kadah, "Determination of the optical properties of a two-layer tissue model by detecting photons migrating at progressively increasing depths," *Appl. Opt.* **42**(31), 6398–6411 (2003).

73. G. Yu, T. Durduran, D. Furuya, J. H. Greenberg, and A. G. Yodh, "Frequency-domain multiplexing system for <emph type ="italic">in vivo</emph> diffuse light measurements of rapid cerebral hemodynamics," *Appl. Opt.* **42**, 2931–2939 (2003).

74. Y. Yang, H. Liu, X. Li, and B. Chance, "Low-cost frequency-domain photon migration instrument for tissue spectroscopy, oximetry, and imaging," *Opt. Eng.* **36**(5), 1562–1569 (1997).

75. A. R. Padhani and L. Ollovier, "The RECIST criteria: implications for diagnostic radiologists," *Br. J. Radiol.* **74**, 983-986 (2001).

76. S. G. Patel and J. P. Shah, "TNM staging of cancers of the head and neck: striving for uniformity among diversity," *Ca-Cancer J. Clin.* **55**(4), 242–258 (2005).

77. A. F. Devries, J. Griebel, C. Kremser, W. Judmaier, T. Gneiting, A. Kreczy, D. Ofner, K. P. Pfeiffer, G. Brix, and P. Lukas, "Tumor microcirculation evaluated by dynamic magnetic resonance imaging predicts therapy outcome for primary rectal carcinoma," *Cancer Res.* **61**(6), 2513–2516 (2001).

78. P. Sonveaux, A. Brouet, X. Havaux, V. Gregoire, C. Dessy, J. L. Balligand, and O. Feron, "Irradiation-induced angiogenesis through the up-regulation of the nitric oxide pathway: implications for tumor radiotherapy," *Cancer Res.* **63**(5), 1012–1019 (2003).

79. M. F. Milosevic, A. W. Fyles, and R. P. Hill, "The relationship between elevated interstitial fluid pressure and blood flow in tumors: a bioengineering analysis," *Int. J. Radiat. Oncol., Biol., Phys.* **43**(5), 1111–1123 (1999).

80. R. E. Meyn, L. C. Stephens, D. W. Voehringer, M. D. Story, N.

Mirkovic, and L. Milas, "Biochemical modulation of radiation-induced apoptosis in murine lymphoma cells," *Radiat. Res.* **136**(3), 327–334 (1993).

81. K. Pietras, K. Rubin, T. Sjoblom, E. Buchdunger, M. Sjoquist, C. Heldin, and A. Ostman, "Inhibition of PDGF receptor signaling in tumor stroma enhances antitumor effect of chemotherapy," *Cancer Res.* **62**(19), 5476–5484 (2002).

82. K. Pietras, M. Stumm, M. Hubert, E. Buchdunger, K. Rubin, C. H. Heldin, P. McSheehy, M. Wartmann, and A. Ostman, "Sti571 enhances the therapeutic index of epothilone b by a tumor-selective increase of drug uptake," *Clin. Cancer Res.* **9**(10,1), 3779–3787 (2003).

83. G. Griffon-Etienne, Y. Boucher, C. Brekken, H. D. Suit, and R. K. Jain, "Taxane-induced apoptosis decompresses blood vessels and lowers interstitial fluid pressure in solid tumors: clinical implications," *Cancer Res.* **59**(15), 3776–3782 (1999).

84. F. Zywietz, W. Reeker, and E. Kochs, "Tumor oxygenation in a transplanted rat rhabdomyosarcoma during fractionated irradiation," *Int. J. Radiat. Oncol., Biol., Phys.* **32**(5), 1391–1400 (1995).

85. A. O. Badib and J. H. Webster, "Changes in tumor oxygen tension during radiation therapy," *Acta Radiol.: Ther., Phys., Biol.* **8**(3), 247–257 (1969).

86. P. Bergsjo and J. C. Evans, "Oxygen tension of cervical carcinoma during the early phase of external irradiation. II. Measurements with bare platinum micro electrodes," *Scand. J. Clin. Lab. Invest.* **27**(1), 71–82 (1971).

87. M. Tomoi, M. Maeda, M. Yoshida, H. Yamada, and Y. Hawamura, "Assessment of radiotherapeutic effect on brain tumors by dynamic susceptibility contrast MRI: a preliminary report," *Radiat. Med.* **17**, 195–199 (1999).

88. A. Makris, T. J. Powles, S. Kakolyris, M. Dowsett, S. E. Ashley, and A. L. Harris, "Reduction in angiogenesis after neoadjuvant chemoendocrine therapy in patients with operable breast carcinoma," *Cancer* **85**, 1996–2000 (1999).

89. V. Ntziachristos, A. G. Yodh, M. Schnall, and B. Chance, "Concurrent MRI and diffuse optical tomography of breast after indocyanine green enhancement," *Proc. Natl. Acad. Sci. U.S.A.* **97**(6), 2767–2772 (2000).

90. N. Shah, J. Gibbs, D. Wolverton, A. Cerussi, N. Hylton, and B. J. Tromberg, "Combined diffuse optical spectroscopy and contrast-enhanced magnetic resonance imaging for monitoring breast cancer neoadjuvant chemotherapy: a case study," *J. Biomed. Opt.* **10**(5), 51503 (2005).